2018 IEEE/RSJ International Conference on Intelligent Robots and Systems (IROS)
Madrid, Spain, October 1-5, 2018

System Identification and Closed-Loop Control of a Hydraulically Amplified Self-Healing Electrostatic (HASEL) Actuator

Cosima Schunk[1] †, Levi Pearson[1†*], Eric Acome[1], Timothy G. Morrissey[1],
Nikolaus Correll[1], Christoph Keplinger[1], Mark E. Rentschler[1,2] and J. Sean Humbert[1]

***Abstract*— This paper describes a system identification method and the development of a closed-loop controller for a Hydraulically Amplified Self-healing ELectrostatic (HASEL) actuator. Our efforts focus on developing a reliable and consistent way to identify system models for these soft robotic actuators using high-speed videography based motion tracking. Utilizing a mass-spring-damper model we are able to accurately capture the behavior of a HASEL actuator. We use the resulting plant model to design a Proportional-Integral controller that demonstrates improved closed-loop tracking and steady-state error performance.**

I. INTRODUCTION

Soft robotics is a rapidly emerging field with widespread applications in health care, robotics industry, and human-machine interactions [1]. Made from flexible or stretchable materials, soft robots are inherently adaptable and can conform to their surroundings without damaging them [1], [2]. Soft actuators are attractive for their low cost, versatility, and performance [3]. While positional tracking and controls are well understood concepts for traditional robots [4], the control of soft robotic systems is nascent field with many opportunities for research and development [5], [6]. The hyper-elastic materials of soft robotic systems are nonlinear and can feature infinite degrees of freedom, which poses new challenges for system identification and controller development.

Soft actuators are an integral component of soft robots. Research into soft actuators or artificial muscles is abundant. Two popular approaches have been soft pneumatic actuators and dielectric elastomer actuators (DEAs). Both of these technologies have critical challenges. Pneumatic actuators require a source of high pressure fluid which limits portability, and DEAs are prone to premature electrical failure which limits practical applications.

Recently introduced Hydraulically Amplified Self-healing ELectrostatic (HASEL) actuators seek to solve challenges inherent with pneumatics and DEAs while simultaneously combining the benefits of each technology [3]. HASEL actuators are electrically controlled, can harness fluidic actuation modes, and have self-sensing capabilities. These attributes present an interesting opportunity for developing closed-loop control of soft robots. Previous works have shown modeling and control of fluidic soft actuators [7]–[10] and DEAs [11], [12].

[1]University of Colorado, Boulder
[2]Senior Member, IEEE
*Corresponding author: lepe8156@colorado.edu
†These authors contributed equally to this manuscript.

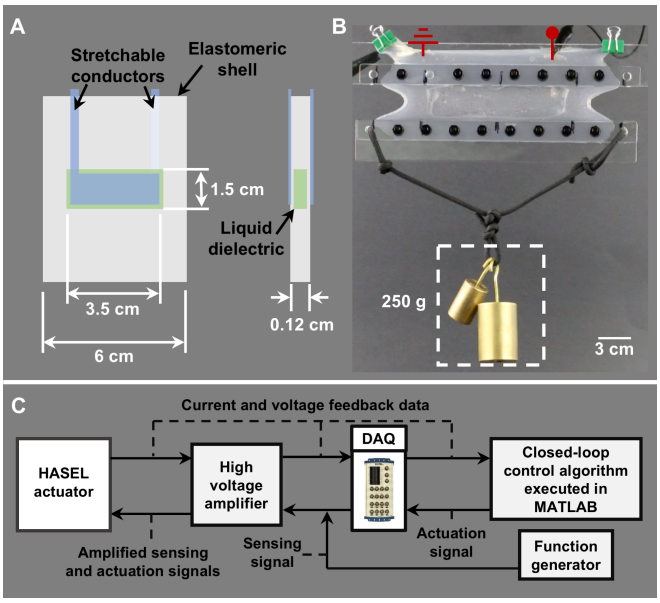

Fig. 1. **A:** A planar HASEL actuator consists of a rectangular elastomeric shell that is filled with a liquid dielectric. Stretchable conductors cover the entire liquid dielectric region. **B:** Both ends of the actuator are laterally pre-stretched onto acrylic clamps and a mass of 0.25 kg is hung from the bottom clamp. **C:** This schematic shows the experimental setup. MATLAB is used to control actuation. The actuator signal is generated in MATLAB and output through a DAQ while a function generator is used to create the low-voltage sensing signal. The sensing and actuation signals are combined before being sent through a high voltage amplifier which is connected to the HASEL actuator. Current and voltage feedback data is measured from the voltage and current monitors of the amplifier and collected through the data acquisition (DAQ) system.

In this work we take first steps toward the development of a robust closed-loop controller for planar HASEL actuators. The planar HASEL actuator has similar function and construction as a DEA. Therefore, we are able to build from existing DEA literature on capacitive self-sensing and controls. In contrast to the exclusively elastomer construction of DEAs, planar HASEL actuators are made from an elastomeric shell filled with a liquid dielectric. The liquid dielectric layer enables self-healing from electrical failure. Additionally, while DEAs, by definition, are made from elastomers, HASEL actuators can be fabricated from a wide range of materials including flexible, yet inextensible polymer films [13]. Linear regions in the stretch-load relationship, where the HASEL behaves like a mass-spring-damper system, were identified through static load tests. In this first approach toward the development of robust closed-

loop controls for a planar HASEL actuator, we limited the dynamics of the actuator to the largest of these linear regions shown in Figure 4). To be able to control the strain of the actuator it is crucial to relate desired strain to required actuation voltage, and sensing voltage to the actual strain achieved. This was accomplished by utilizing high speed video recordings of the actuated HASEL while simultaneously recording actuation and sensing voltages. Once these relationships were established, actuation with a chirp-signal was used to generate a open-loop Bode plot which allowed us to identify the natural response of the system and the limitations of the HASEL actuators. In open-loop actuation a persistent drift between desired and measured strain is present. A Proportional-Integral (PI) controller is implemented to counter this drift and improve tracking performance. The implementation of this controller, was done in MATLAB (R2017a, The MathWorks Inc.).

II. HASEL ACTUATORS

The basic components of a HASEL actuator include a stretchable or flexible shell which is filled with a liquid dielectric as shown in Figure 1. Opposing electrodes are placed on the outside of the shell and applying voltage across the electrodes generates electrostatic forces which act on the insulating liquid and shell. This electro-hydraulic coupling provides a voltage-controlled method for generating force and displacement. A variety of actuation modes and materials can be used to create HASEL actuators with muscle-like performance [3], [13].

The electrodes of HASEL actuators function as parallel plates of a variable capacitor where capacitance, C, relates to the area of the electrodes and thickness of the dielectric between the electrodes as follows:

$$C \propto \frac{A}{d}, \tag{1}$$

where A is the area of the parallel electrodes and d is the total thickness of the liquid and solid dielectric layer between the electrodes. Capacitance of soft electrostatic actuators can be measured during activation by superimposing a high-frequency signal over the actuation signal [14]. The high-frequency sensing signal is at a relatively low voltage and does not influence the actuation response. This ability to self-sense actuation makes it possible to control HASEL actuators without the use of additional sensors [11], [12].

In this paper we characterize and control actuation of a planar HASEL actuators which operates in a similar fashion as planar Dielectric Elastomer Actuators (DEAs). Electrodes cover the entire portion of the liquid dielectric region and when activated, the HASEL actuator reduces in thickness and expands in area. By applying pre-stretch in one direction and a load in the orthogonal planar direction, the planar HASEL actuator will linearly expand in the direction of the load.

The shell of the HASEL actuator used in this work is made from Ecoflex 00-30 (Smooth-On), a highly stretchable silicone elastomer. The electrodes are ionically conductive PAM-LiCl hydrogels made with 8M LiCl solution [15]. Electrodes are bonded to the surface of the silicone elastomer shell by treating the surface with a 10 wt% solution of benzophenone [16]. A thin encapsulating layer of Ecoflex 00-30 is cast over the top of the the electrodes to improve durability. The elastomeric shell is fabricated as two halves then bonded together using uncured Ecoflex 00-30. The center of the shell is left un-bonded and is filled with 0.6 mL of liquid dielectric (Envirotemp FR3, Cargill). Overall thickness of the fabricated actuator before prestretch is 0.12 cm (Figure 1A).

III. EXPERIMENTAL SETUP

To operate as a linear actuator, the HASEL actuator is mounted with 3x pre-stretch in the lateral direction. Pre-stretch is fixed at both ends using clamps made from rectangular acrylic sheets and plastic screws. The top clamp is mounted on a fixed stand and a load is hung from the bottom clamp.

The input signal supplied to the HASEL actuator is a composite of two waveforms. The first waveform is a DC voltage signal which controls the contraction or elongation of the actuator. The second waveform is a sensing signal set at a high frequency and low amplitude, which allows for capacitive self-sensing. The driving voltage signal is generated by a custom MATLAB script, transmitted with a data acquisition board (DAQ) (NI USB-6212, National Instruments Corporation, Austin, Texas USA). The high frequency of the sensing signal (2,000 Hz sine wave) was produced with a function generator (33500B Waveform Generator, Keysight Technology Inc., Santa Rosa, CA USA). The sensing and actuation signals were combined in series and connected to the input of the high-voltage amplifier (Model 50/12, TREK Inc., Lockport, NY USA) which has a gain of 5,000 V/V . The separation of actuation and sensing output signals was necessary because of inherent time delays in the communication between MATLAB and the DAQ, which limit the rate of updated voltage output through the DAQ to 100 Hz.

The TREK provides a voltage and a current monitor signal which are recorded by the DAQ and read at a rate of 200 kHz by the MATLAB program. When the DAQ input buffer reaches 2,000 readings, a new output buffer is created (every 10 ms). Similar to a DEA, the electrical model of a HASEL actuator is a resistor and capacitor in series. Therefore, the voltage and current monitor signals from the TREK can be used to monitor capacitance. To reduce noise of the monitor signals a low-pass filter is applied to both signals (4^{th} order Butterworth filter with a cutoff frequency of 2,001 Hz). Additionally the 20 periods of the sensing sine wave contained in the 10 ms of input buffer are averaged. The phase difference between the voltage and current monitor signal are calculated with a custom MATLAB script, phdiffmeasure.m (Hristo Zhivomirov, MathWorks File Exchange).

Based on these two signals the relative capacitance, C_r, was calculated as follows:

$$X_c = 2.5e^6 \cdot \left\| \frac{V_v}{V_c} \right\| * \sin(|\varphi|), \tag{2}$$

$$C_r = \left\| \frac{1}{X_c \cdot 2\pi \cdot f \cdot 10} \right\|. \tag{3}$$

where X_c is the capacitive reactance, f is the frequency of the sensing signals, φ is the phase difference between the two signals, V_v and V_c are the peak-to-peak amplitudes of the sensing voltage and the current monitor signals from the amplifier, respectively, [14]. The other values in equations (2) and (3) are multipliers to scale the measured signals.

We used correlations established during the system identification process to convert relative capacitance to strain. In the closed-loop condition, the measured strain is compared to a desired strain and the resulting error is used to define a corrected output strain. A correlation between strain and output voltage was then used to convert the corrected output strain to an output voltage.

Preliminary tests where hundreds of particles were automatically tracked (DiaTrack verion 3.05 [17] showed 1D-stretch to be fairly homogeneous across the length of the actuator but lateral displacement was observed in the unconstrained areas away from the mid-line. With the goal of controlling total elongation in one direction only, it was determined that tracking of particles at the lower clamp, where displacement is largest and where the least lateral displacement occurs, would yield sufficient accuracy for our purposes. Therefore, we manually tracked three points in that region using the Manual Tracking plug-in of the ImageJ Fiji package [18] and used the average strain changes based of these three points for the following system identification process.

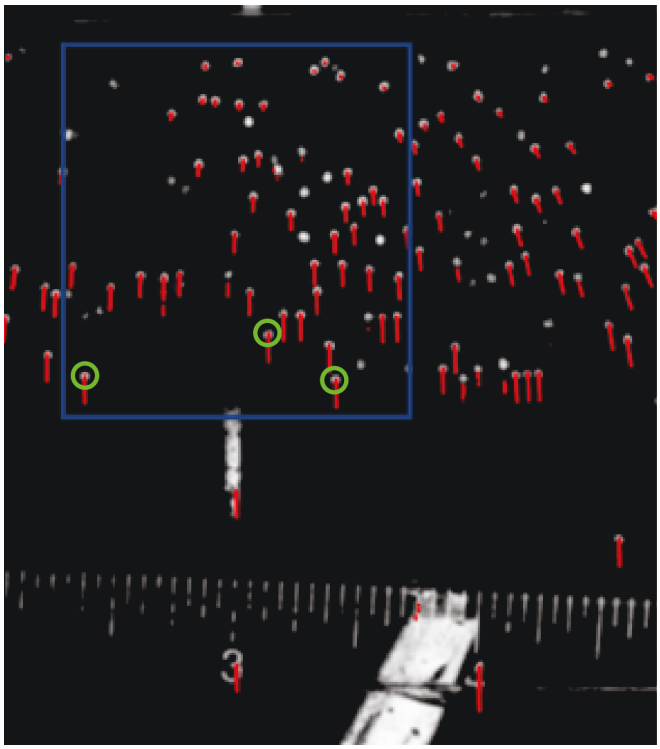

Fig. 2. Results of the auto-tracking function used in Diatrack. Larger and more homogeneous strain paths are shown the closer to the bottom of the actuator. Sideways movement is seen on the far right of the image, indicating stretch in the horizontal direction in unconstrained areas of the actuator. The center line is indicated by the white line on the bottom clamp. Particles chosen for manual tracking highlighted with green circles.

IV. System Identification Process

A. Establishing I/O relationships

To establish the relationship between actuation voltage and desired strain, as well as actual strain and relative capacitance, the actuator was fed a triangular input signal with a range from 0 V to 2 V (0 V to 10 kV after amplification in the TREK) and a frequency of 0.25 Hz. Running at 400 Hz and full resolution the camera captured five cycles of actuation over 20 s Voltage and capacitance were recorded simultaneously. The visco-elastic properties of the elastomeric outer layer of the HASEL actuator cause the sensed strain to never return to zero percent strain after the first triangle wave is sent. The remaining four cycles do show repeatable strain measurements (figure 3A).

Both the voltage-strain and the strain-capacitance relationships contained a hysteresis band. To relate input voltage, V_{input}, to desired strain, ϵ_{des}, we used the MATLAB Curve Fitting app to fit a sum of two exponentials to the hysteresis loop (Figure 3B):

$$V_{input} = 1.324e^{3.124\cdot\epsilon_{des}} - 0.2805e^{-26.92\cdot\epsilon_{des}}. \quad (4)$$

To obtain a fit for the strain-capacitance relationship we averaged the strain of the rising and falling edge of the strain-time and capacitance-time curve and used a linear fit in the Curve Fitting application (Figure 3C).

$$\epsilon_{cap} = 4.923e^{6}C_{rel} - 0.276. \quad (5)$$

B. Static tests

Although the final goal is the development of non-linear controls for the planar HASEL actuator, the first step is reliable linear control. Knowing that we can expect non-linearities from the material properties of the elastomeric shell, a static load test was conducted. Comparing the applied load to the corresponding amount of elongation. The Arruda and Boyce model was chosen for this test because of its ability to accurately capture the force-to-stretch relationships in elastomeric materials [19]. The linear region of the stress was identified using piecewise linear fits. The determined linear region is highlighted in yellow and shown in Figure 4.

C. Defining the linear system

Based on the results from the previous two sections, we decided on a system that is loaded with a mass of 0.25 kg and supplied with a 5 kV baseline voltage. The mass-loading ensures that the baseline strain is centered in the longest linear region identified in the static test (Figure 4). The baseline voltage allows for negative and positive strain around the set point. If the baseline voltage were to be 0 kV, the system would only undergo elongation if actuated. By operating at the baseline voltage the actuator can now be contracted, by lowering the applied voltage, or elongated by applying higher voltages.

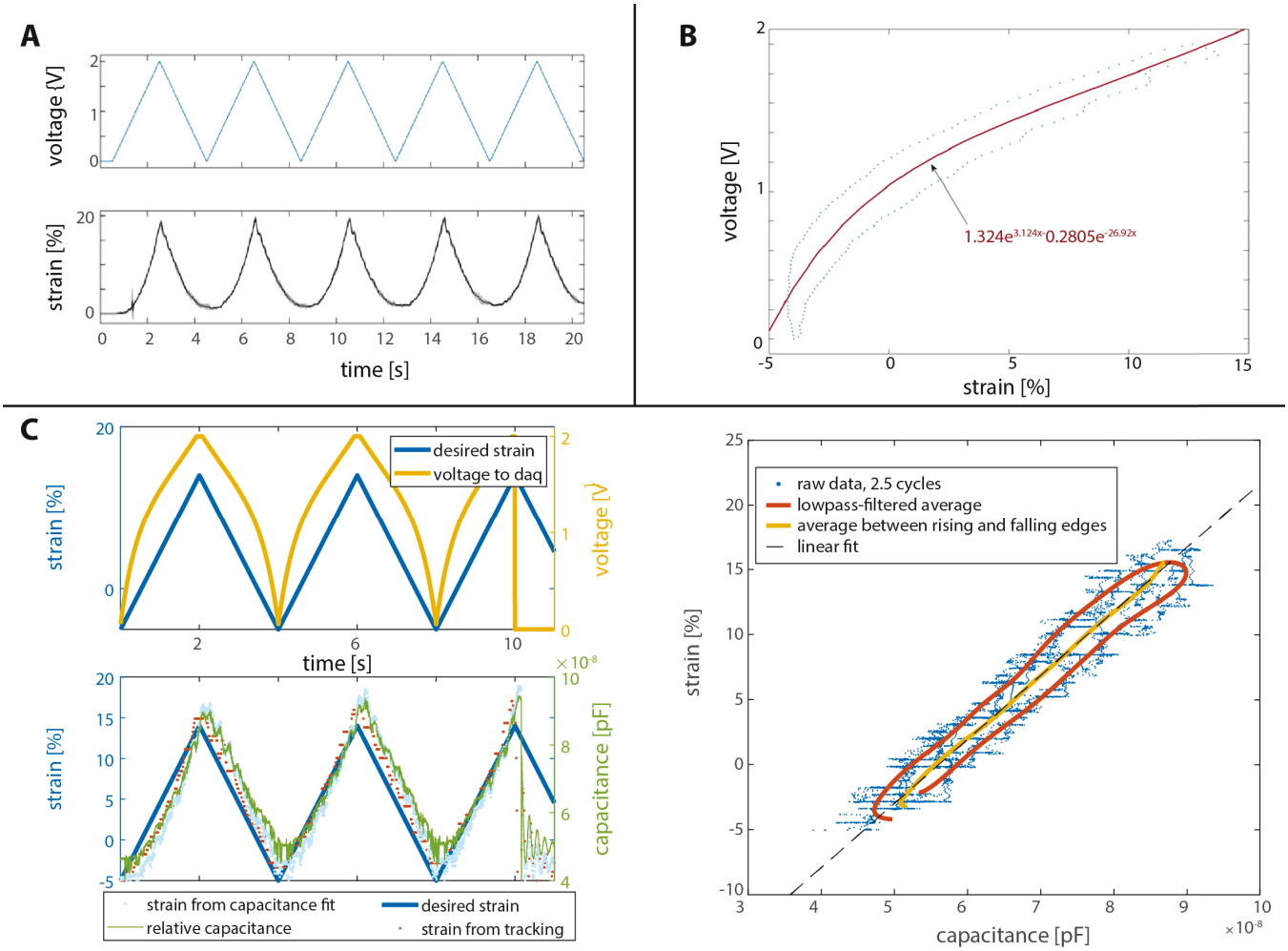

Fig. 3. Results for correlation between DAQ output voltage, strain and capacitance. The DAQ output voltage is amplified by a factor of 5000 by the TREK to provide the required high voltage for the HASEL. **A:** Traces of DAQ output voltage over time (top) and average strain based on marker tracking (bottom). **B:** Exponential fit for voltage to strain relationship. Note that the reference 0 % strain is shifted with respect to subplot A to reflect the chosen baseline voltage of 5 kV as reference for the strain. **C:** Correlation of capacitance to strain. On the left, applied DAQ output voltage for desired strain (upper panel), strain from tracking, capacitance and reconstructed strain vs. time (lower panel). On the right, linear fit of capacitance to averaged strain measurements.

D. Dynamic tests

We performed dynamic tests to further characterize our system. We lifted the 0.25 kg mass, allowing the actuator to return to its unloaded state, and then suddenly loaded the actuator with the mass. This free response of the actuator was recorded with the high-speed camera. The tracked marker traces were converted into elongation change, dt, and exported to MATLAB.

Equation 6 is used to find the damped natural frequency, ω_d, and the exponential decay rate, δ, of the system

$$\Delta x = Ae^{-\delta t}\cos\left(\omega_d t - \varphi_0\right), \tag{6}$$

where Δx is the length change, A the amplitude, t the time, and φ the phase. The natural frequency, ω_0, is related to the damped natural frequency and exponential decay as follows:

$$\omega_0 = \sqrt{\omega_d^2 + \delta^2}. \tag{7}$$

Figure 5 shows the displacement trace of two separate trials conducted with the following baseline parameters: an applied voltage of 5 kV and a 0.25 kg mass. The fit of equation 6 is not shown, but the natural frequency of that fit was $\omega_d = 5.1\ rad/s$. The hull curves between the positive and negative peaks were asymmetrical with exponential decay rates of -3.6 and -4.2 respectively. The natural frequency computes to be $\omega_0 = 5.1\ rad/s$ in both cases. This result will serve as validation for the Bode plot described in the following section.

V. Controller Design

This section discusses the empirical estimation of the open-loop Bode plot of the HASEL actuator and design of a PI controller to improve tracking performance. To generate the open-loop Bode plot, a chirp signal was applied that oscillated about the 5 kV baseline voltage with ±3 kV. The chirp had a duration of 10 s, with frequncing increasing linearly from 0.1 Hz to 10 Hz. The resulting input-output signals yielded the following transfer function:

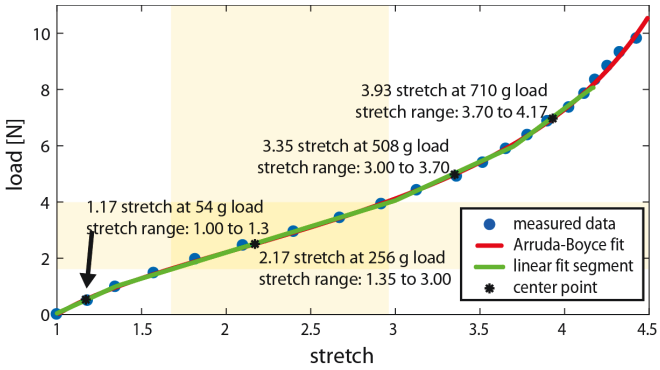

Fig. 4. Results of the static tests. The measured load-stretch data points are shown in blue, the fit based on the Arruda-Boyce model is shown in red, linear regions are represented as green lines with their center points indicated by black asterisks. The region we chose for the experiments is indicated in with yellow overlays..

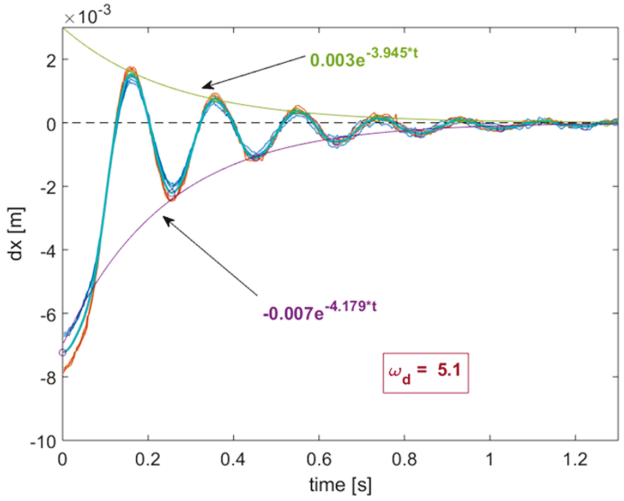

Fig. 5. The displacement vs. time traces of two trials are shown in blue and red, respectively. The shaded are of these two traces shows the standard deviation of the average of three individually tracked and then averaged particle traces. The light blue line is the mean between these two trial. The hull curves using the positive and negative peaks are shown in green and purple, respectively, with the corresponding equations

$$G(s) = \frac{1}{2}\frac{26.14}{s^2 + 0.93s + 26.14}. \tag{8}$$

Equation 8 is the model transfer function that is used for our controller design. This transfer function is an acceptable fit because of its similar natural resonance peak and response to input stimuli. However, it does lack more complicated non-linearities present in the lower and higher stretch regions shown in Figure 4 and non-linear behaviors such as elastic recoil. Therefore, the goal of this controller is to improve steady state tracking error already present in the system.

From the second order transfer function the following system parameters are found:

$$\omega_n = 5.11\ rad/s, \tag{9}$$

$$\zeta = 0.09. \tag{10}$$

To improve the tracking error, a PI controller is implemented to reduce the rise-time and steady-state error by adding gain at low frequencies [20]. The proportional term reduces rise time because it directly impacts the overall gain of the system and increases the crossover frequency [20]. However, this does worsen the overshoot by decreasing the damping ratio of the system. The integral term in the controller serves the purpose of reducing the steady state error present in the plant [20]. The proportional and integral terms are summed up in the following frequency domain equation:

$$K_p + \frac{K_i}{s} = \frac{K_p s + K_i}{s}. \tag{11}$$

Equation 11 creates the ability to edit the poles and zeros of the controller based on what values are chosen for K_p and K_i. The gains of the controller were selected based on the desired shape of the open-loop bode plot, and fine-tuned manually. Gain selection was guided by the desire to increase the magnitude at low frequencies while at least maintaining the crossover frequency of the open-loop plant. The limitations of this controller are not rooted in the demand placed on the actuator input, but rather, failure by dielectric breakdown [21]. A saturation limit of $-0.05 \leq u(t) \leq 0.1$, where $u(t)$ is the input strain, will be implemented to eliminate the possibility of the HASEL actuator failing due to dielectric breakdown [21].

$$K_p = 0.85, \tag{12}$$

$$K_i = 1.5. \tag{13}$$

The resulting Bode plot for the loop transfer function is shown in 7. The upward shift in the slope for lower frequencies corresponds to improved tracking, while the increased crossover frequency indicates a faster rise time.

VI. Results

Generating and sending a step response to the system in both open and closed loop configurations allowed for a side by side comparison of each system. In Figure 6 an initial step input is applied to put the actuator at the predefined zero strain state. After that, a traditional step input is applied to the system. The natural plant responds to a step input with an finite steady state error and a slow rise time. The cause of the finite steady state error is viscoelastic creep. As weight hangs from the HASEL actuator it causes deformation over time causing drift in the system. The controller design accounts for this drift using the integral term of the controller. The affect of the controller is shown in Figure 6. The second benefit of the controller is a decrease in rise time. Prior to controller implementation the rise time is approximately 6-8 s. With closed-loop control this value is reduced to a range of 2.5-3 s. This decrease in response time is a result of the proportional term in the controller.

‘

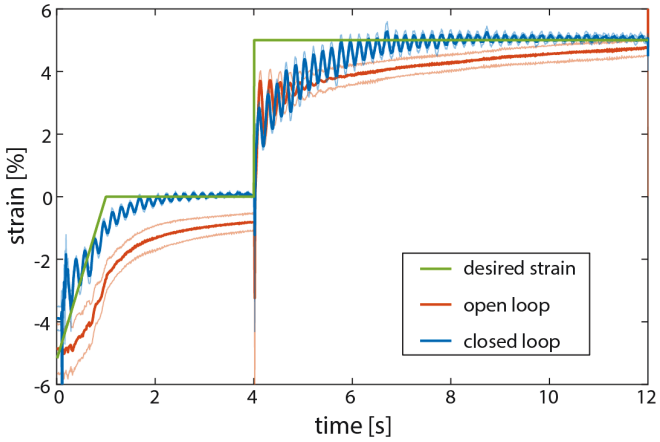

Fig. 6. Empirical results. Desired strain (green) open loop (red) and closed loop (blue) step responses over time. The thick lines are the average of six and four trials for the open and closed loop, respectively. The faint lines show the respective standard deviations for the open loop tests only.

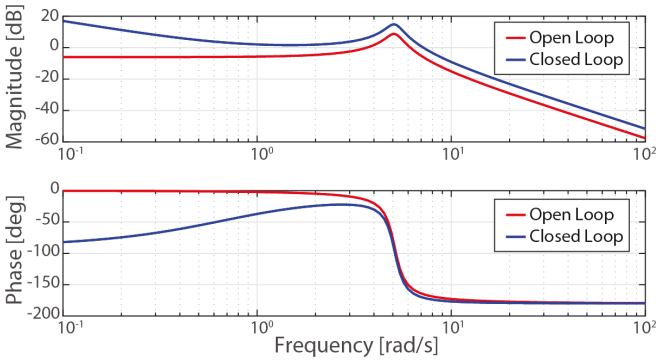

Fig. 7. Comparison between open (red) and closed loop (blue) Bode plot.

VII. Discussion

Results show that a simple spring-mass model and appropriate system identification lead to acceptable performance under closed-loop control within a well-defined strain region which is important for using this novel kind of actuator in robotic applications. To make this actuator more applicable for robotic applications the oscillatory behavior must be addressed. This can be mediated by introducing a derivative term into the PI controller and will be part of future efforts. We are furthermore switching to an ATmega2560 based controller that allows for faster update times for the controller.

Planar HASEL actuators show non-linear behavior due to the properties of its elastomeric shell. A possible way to address this issue is by implementing a hybrid controller. The relationship between the mass and stretch is a reliable way to tell whether or not the actuator is in the linear region of stretch. Sensing the weight hung from the actuator can indicate whether a linear or non-linear controller must be used.

This setup required a large amount of bench top equipment. These pieces of equipment are used to generate the required actuation voltage, measure the self-sensing capacitance, and carry out closed-loop control. To integrate HASEL actuators into compact robotic systems these components must be miniaturized. This is possible with off-the-shelf components. For example the Peta-Pico Voltron project[1], and miniature digital signal processing devices that can perform the required phase shift calculations at high speeds.

VIII. Conclusion

We have performed system identification and developed a controller for a planar HASEL actuator. To this end, we have described a complete system that includes high voltage generation, state estimation, signal processing and control, which can serve as a blueprint for further miniaturization and integration into a self-contained actuator. This is the first example of closed-loop control with a HASEL actuator and in the future we hope to expand our controls to include non-linear regions of the planar HASEL actuators. Additionally, a key strength of HASEL actuators is the ability to produce a variety of actuation modes with different designs and geometries. While the closed-loop control demonstrated here is applicable for only one design of HASEL actuator, future work will explore control of different HASEL actuator designs and aim to develop a general transfer function.

Acknowledgment

Our funding comes from the NSF Cyber-Physical Systems grant No. 1739452. We thank Angela Maio for her help in troubleshooting the communication scripts with the NI data acquisition board. We thank Shane Mitchell, Nick Kellaris, Khoi Ly and Mantas Naris for scientific discussions and helpful input.

References

[1] C. Majidi, "Soft robotics: A perspective-current trends and prospects for the future," *Soft Robotics*, vol. 1, no. 1, pp. 5–11, 2013.

[2] S. Bauer, S. Bauer-Gogonea, I. Graz, M. Kaltenbrunner, C. Keplinger, and R. Schwdiauer, "25th anniversary article: A soft future: From robots and sensor skin to energy harvesters," *Advanced Materials*, vol. 26, no. 1, pp. 149–162, 2014. [Online]. Available: http://dx.doi.org/10.1002/adma.201303349

[3] E. Acome, S. Mitchell, T. Morrissey, M. Emmett, C. Benjamin, M. King, M. Radakovitz, and C. Keplinger, "Hydraulically amplified self-healing electrostatic actuators with muscle-like performance," *Science*, vol. 359, no. 6371, pp. 61–65, 2018.

[4] B. C. McInnis and C.-K. Frank Liu, "Kinematics and dynamics in robotics: A tutorial based upon classical concepts of vectorial mechanics," vol. 2, pp. 181 – 187, 01 1987.

[5] M. Calisti, M. Giorelli, G. Levy, B. Mazzolai, B. Hochner, C. Laschi, and P. Dario, "An octopus-bioinspired solution to movement and manipulation for soft robots," *Bioinspiration & Biomimetics*, vol. 6, no. 3, p. 036002, 2011. [Online]. Available: http://stacks.iop.org/1748-3190/6/i=3/a=036002

[6] G. Robinson and J. Davies, "Continuum robots-a state of the art," vol. 4, pp. 2849 – 2854 vol.4, 02 1999.

[7] P. Polygerinos, N. Correll, S. A. Morin, B. Mosadegh, C. D. Onal, K. Petersen, M. Cianchetti, M. T. Tolley, and R. F. Shepherd, "Soft robotics: Review of fluid-driven intrinsically soft devices; manufacturing, sensing, control, and applications in human-robot interaction," *Advanced Engineering Materials*, 2017.

[8] A. D. Marchese and D. Rus, "Design, kinematics, and control of a soft spatial fluidic elastomer manipulator," *The International Journal of Robotics Research*, vol. 35, no. 7, pp. 840–869, 2016.

[1] http://petapicovoltron.com/

[9] A. D. Marchese, R. Tedrake, and D. Rus, "Dynamics and trajectory optimization for a soft spatial fluidic elastomer manipulator," *The International Journal of Robotics Research*, vol. 35, no. 8, pp. 1000–1019, 2016.

[10] C. M. Best, M. T. Gillespie, P. Hyatt, M. Killpack, L. Rupert, and V. Sherrod, "Model predictive control for pneumatically actuated soft robots," *IEEE Robotics & Automation Magazine*, vol. 2, no. 9, p. 31, 2016.

[11] G. Rizzello, D. Naso, A. York, and S. Seelecke, "Closed loop control of dielectric elastomer actuators based on self-sensing displacement feedback," *Smart Materials and Structures*, vol. 25, no. 3, p. 035034, 2016. [Online]. Available: http://stacks.iop.org/0964-1726/25/i=3/a=035034

[12] B. M. O. Todd A. Gisby and I. A. Anderson, *Applied Physics Letters*, vol. 102, 2013.

[13] N. Kellaris, V. G. Venkata, G. M. Smith, S. K. Mitchell, and C. Keplinger, "Peano-hasel actuators: Muscle-mimetic, electrohydraulic transducers that linearly contract on activation," *Science Robotics*, vol. 3, no. 14, p. eaar3276, 2018.

[14] C. Keplinger, M. Kaltenbrunner, N. Arnold, and S. Bauer, "Capacitive extensometry for transient strain analysis of dielectric elastomer actuators," *Applied Physics Letters*, vol. 92, no. 19, p. 192903, 2008.

[15] F. X. J. Z. H. W. Yuanyuan Bai, Baohong Chen and Z. Suo, "Transparent hydrogel with enhanced water retention capacity by introducing highly hydratable salt," vol. 105, 2014. [Online]. Available: http://aip.scitation.org/doi/10.1063/1.4898189

[16] Z. T. L. S. P. G. A. Z. X. Yuk, Hyunwoo, "Tough bonding of hydrogels to diverse non-poroussurfaces," *Nature Materials*, vol. 15, pp. 190–196, 2015.

[17] P. Vallotton and S. Olivier, "Tri-track: Free software for large-scale particle tracking," *Microscopy and Microanalysis*, vol. 19, no. 2, p. 451460, 2013.

[18] J. Schindelin, I. Arganda-Carreras, and E. Frise, "Fiji: an open-source platform for biological-image analysis," *Nature methods*, vol. 9, pp. 676–682, 2012.

[19] E. M. Arruda and M. C. Boyce, "A three-dimensional constitutive model for the large stretch behavior of rubber elastic materials," *Journal of the Mechanics and Physics of Solids*, vol. 41, no. 2, pp. 389–412, 1 1993.

[20] B. Messner, D. Tilbury, R. Hill, and J. Taylor. (2011) Control Tutorials for MATLAB & Simulink kernel description. [Online]. Available: http://ctms.engin.umich.edu/CTMS/index.php?aux=Home

[21] J.-S. Plante and S. Dubowsky, "Large-scale failure modes of dielectric elastomer actuators," *International Journal of Solids and Structures*, vol. 43, no. 25, pp. 7727 – 7751, 2006. [Online]. Available: http://www.sciencedirect.com/science/article/pii/S0020768306000990